https://doi.org/10.1016/j.aca.2021.339070

Measurement error due to self-absorption in calibration-free laser- induced breakdown spectroscopy

Aya Taleb [a, b], Vincent Motto-Ros [c], Mauro J. Carru [a], Emanuel Axente [d], Valentin Craciun [d], Frederic Pelascini [b], Jörg Hermann [a, *]

[a] *Aix-Marseille University, CNRS, LP3, 13288, Marseille, France*

[b] *Cetim Grand Est, 67400, Illkirch-Graffenstaden, France*

[c] *University Lyon 1, CNRS, Institut Lumi'ere Mati'ere, 69622, Villeurbanne, France*

[d] *National Institute for Laser, Plasma and Radiation Physics, 77125, Măgurele, Romania*

* Corresponding author.
E-mail address: jorg.hermann@univ-amu.fr (J. Hermann).

Keywords:
Elemental analysis
Laser-induced breakdown spectroscopy Calibration-free
Self-absorption Error evaluation

Abstract

Self-absorption of spectral lines is known to lower the performance of analytical measurements via calibration-free laser-induced breakdown spectroscopy. However, the error growth due to this effect is not clearly assessed.

Here we propose a method to quantify the measurement error due to self-absorption based on the calculation of the spectral radiance of a plasma in local thermodynamic equilibrium. Validated through spectroscopic measurements for a binary alloy thin film of compositional gradient, the method evidences that measurement performance lowering due to self-absorption depends on the spectral shape of the analytical transition and on the intensity measurement method. Thus, line-integrated intensity mea- surements of Stark broadened lines enable accurate analysis, even at large optical thickness, if line width and plasma size are precisely known. The error growth due to self-absorption is significantly larger for line shapes dominated by Doppler broadening and for line-center intensity measurements. The findings present a significant advance in compositional measurements via calibration-free laser-induced break- down spectroscopy, as they enable straightforward selection of most appropriate analytical lines.

1. Introduction

Self-absorption is well-known in plasma diagnostics as it alters the intensity and the spectral shape of transitions [1]. The effect takes place when photons have non-negligible probability of being reabsorbed within the plasma. Self-absorption is thus significant in large-size or high-density plasmas, when the characteristic length of absorption is comparable to the plasma size, or smaller. This is typically the case for lines emitted from laser-induced plasmas, due to the large plasma density [2]. Self-absorption is therefore a major issue in material analysis via calibration-free laser-induced breakdown spectroscopy (LIBS), where the effect is considered as the principal error source of the analytical measurement [3].

Thus, methods for the evaluation and compensation have been proposed [4,5]. Several authors report calibration-free LIBS measurements in optically thin conditions, choosing transitions for which self-absorption is negligible [6,7]. Other authors propose correction methods that enable analytical measurements with even strongly self-absorbed lines [8,9]. These approaches seem to be in opposition with the “golden rule” in plasma diagnostics, that recommends to use transitions of moderate optical thickness only (t _ 1), for which accurate corrections of intensity or width measurements are guaranteed [10].

Despite investigations of calibration-free LIBS measurement errors [11], and the great recent interest in the role of selfabsorption [12e15], accuracy lowering due to the effect has not been yet assessed, and the choice of the most appropriate analytical lines still remains arbitrary. Her ewe propose a method to evaluate the growth of the analytical measurement error due to self-absorption, based on the mostly applied physical model of a uniform plasma in local thermodynamic equilibrium (LTE). The error evaluation has validity not only for our calibration-free approach that intrinsically accounts for selfabsorption, but for all approaches based on the uniform LTE plasma with appropriate self-absorption correction. The fundamentals of the error evaluation are described in the next section, followed by the illustration of the validation through analytical measurements of a binary alloy thin film of variable elemental composition.

2. Materials and methods

2.1. Fundamentals

2.1.1. Analytical signal dependence on optical thickness

The spectral radiance of a uniform plasma in LTE is given by [16].

$$B_\lambda(\lambda) = B_\lambda^0(1 - e^{-\tau(\lambda)}), \qquad (1)$$

where B0l is the blackbody spectral radiance and l is the wavelength. The optical thickness is given by t ¼ !a(z)dz ¼ aL, where a is the absorption coefficient and L is the plasma size along the line of sight. The absorption coefficient of a spectral line is given by [17].

$$\alpha(\lambda) = \pi r_0 \lambda^2 f_{lu} n_l P(\lambda)\left(1 - e^{-hc/\lambda kT}\right), \qquad (2)$$

where r0 is the classical electron radius, h is the Planck constant, c is the vacuum light velocity, k is the Boltzmann constant, T is the temperature, flu is the absorption oscillator strength of the transition, and P(l) is the normalized line profile. The lower level population number density nl is related to the number density of the emitting species via the Boltzmann law, and to the atomic number density of the element via the set of Saha-equations (see SM 1.1). To compare measured and computed spectra, the spectral radiance computed according to eq (1) is convoluted with the apparatus spectral profile), wheras the measured intensity is corrected by the apparatus response. Thus, the corrected measured intensity is

$$I(\lambda) = \int_0^\infty P_{ap}(\lambda - \lambda') B_\lambda(\lambda')\, d\lambda'. \qquad (3)$$

Introducing the line-center optical thickness $\tau_0 = \tau(\lambda_0)$, we can compute the intensity as a function of τ_0, as shown in Fig. 1 for the line-center intensity I_0 and spectrally integrated line intensities I_{line} of different line shapes. Note that I_{line} equals the line-integrated spectral radiance and the corresponding curves are therefore independent of the apparatus spectral width w_{ap}. Contrarily, I_0 equals the line-center spectral radiance only, if w_{ap} is small compared to the line width w. The saturation of I_0, observed for $\tau_0 \simeq 3$, is therefore shifted towards larger t0-values, if the condition $w_{ap} \ll w$ is not fulfilled (see SM 1.2). The weakest and strongest influence of self-absorption on Iline is observed for Lorentzian and Gaussian line profiles, respectively.

The difference is due to the smaller line wings of the Gaussian profile (see SM 1.2). The influence of self-absorption on I_{line} gradually diminishes with increasing Lorentzian contribution. All line profiles with a Lorentzian contribution show an intensity increase $I_{line} \propto \sqrt{\tau 0}$ at the limit of large self-absorption, in agreement with the observations of Gornushkin et al. [18].

2.1.2. Error evaluation

2.1.2.1. Optically thin case. In case of negligible absorption ($t \ll 1$), eq (1) becomes

$$B_\lambda(\lambda) = \epsilon_{ul}\, P(\lambda)\, L, \qquad (4)$$

with the emission coefficient

$$\epsilon_{ul} = \frac{hc}{4\pi\lambda} A_{ul}\, n_u. \qquad (5)$$

Here, A_{ul} is the Einstein coefficient of spontaneous emission, and n_u is the upper level population number density. Substituting n_u in eq (5) by the atomic number density of the element n_A (see SM 1.1), we obtain from eqs (3)-(5)

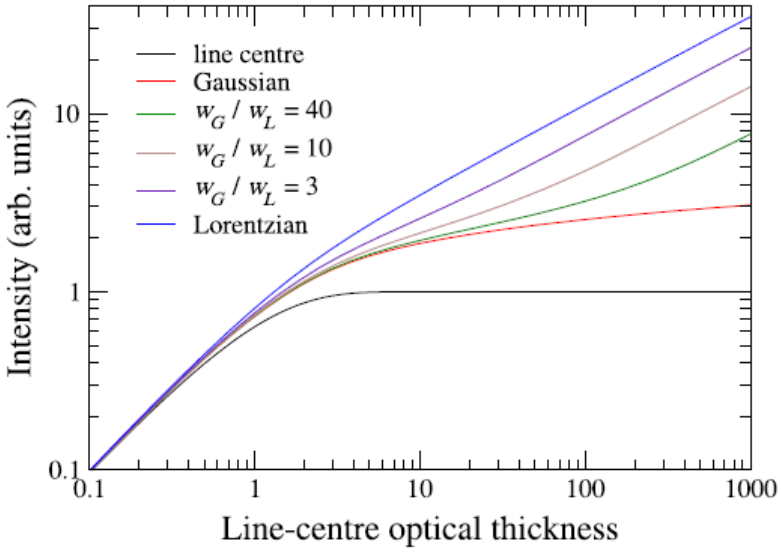

Fig. 1. Intensity vs t0 computed according eq (1): line-center intensity (black curve) and line-integrated intensities (colored curves) for line profiles with different ratios of Gauss width w_G over Lorentz width w_L.

$$n_A = \Theta_1(T, n_e)\frac{I_{line}}{A_{ul}L} \simeq \Theta_1(T, n_e)\frac{I_0\, w_m}{A_{ul}L}, \quad (6)$$

where w_m is the measured line width and Θ_1 is a function of temperature T and electron density n_e that comprises all

$$\frac{\Delta n_A}{n_A} = \sqrt{\left(\frac{\Delta I}{I}\right)^2 + \left(\frac{\Delta A_{ul}}{A_{ul}}\right)^2}, \quad (7)$$

constants including a spectral-shape-dependent correction factor to be applied to I_0 x w_m to obtain the line-integrated intensity. Neglecting errors associated to Θ_1, the error of the atomic number density is
with $\Delta I/I = \Delta I_m/I_m$ for line-integrated measurements. In case of line center intensity measurements, we have

$$\frac{\Delta I}{I} = \sqrt{\left(\frac{\Delta I_0}{I_0}\right)^2 + \left(\frac{\Delta w_m}{w_m}\right)^2}. \quad (8)$$

According to eq (4), a change of L will alter the intensity of all optically thin lines by the same factor. As calibration-free LIBS is based on measurements of relative intensities, the uncertainty of L does not impact the analysis and DL is ignored in eq (7). Thus, disregarding the errors associated to Q1 (T and ne measurements and LTE model calculations), the analytical measurement using an optically thin line has two main error contributions: (i) The intensity measurement error including the uncertainty of the apparatus response function, and (ii) the uncertainty of the transition probability.

2.1.2.2. General case. Substituting n_I by the atomic number density of the element, we obtain from eq (2) after integration over the line profile (see SM 1.3)

$$n_A = \Theta_2(T, n_e)\frac{\tau_0\, w_{sd}}{A_{ul}L}, \quad (9)$$

where Θ_2 is a function of Tand n_e, and w_{sd} is the spectral width of the line due to Stark and Doppler broadening. Neglecting uncertainties associated to Θ_2, the error of the atomic number density is

$$\frac{\Delta n_A}{n_A} = \sqrt{\left(\frac{\Delta \tau_0}{\tau_0}\right)^2 + \left(\frac{\Delta A_{ul}}{A_{ul}}\right)^2 + (1-e^{-\tau_0})\left(\left(\frac{\Delta w_{sd}}{w_{sd}}\right)^2 + \left(\frac{\Delta L}{L}\right)^2\right)}. \quad (10)$$

Here, the factor $1\text{-}e^{-\tau}$ is inserted empirically to retrieve the expression for the optically thin case [eq (7)] for $\tau_0 \ll 1$. The error $\Delta\tau_0$ is obtained from the $I = f(\tau_0)$ dependence displayed in Fig. 1 via the derivative of the inverse function. We have

$$\frac{\Delta \tau_0}{\tau_0} = \frac{1}{\tau_0}\frac{f(\tau_0)}{f'(\tau_0)}\frac{\Delta I}{I} \equiv g(\tau_0)\frac{\Delta I}{I}, \quad (11)$$

where f0(t0) $\equiv$ vI/vt0. The error growth factor g(t0) is introduced to account for the increase of measurement uncertainty due to selfabsorption. For line-center intensity measurements, the error growth factor is obtained in case of negligible apparatus broadening directly from eq (1) as

$$g_0 = \frac{1-e^{-\tau_0}}{\tau_0\, e^{-\tau_0}}. \quad (12)$$

For measurements of the line-integrated intensity, no analytical expression $I_{line} = f(\tau_0)$ exists for common line shapes represented by the Voigt profile. The error growth factor is thus obtained from eq (11) using the numerically calculated derivative $f'(\tau_0)$.

According to the $I_{line}(\tau_0)$-dependence shown in Fig. 1, a moderate error growth by $g \leq 2$ is observed for the Lorentzian line shape (see Fig. 2). The error increases with the Gaussian contribution to the line profile. However, the error amplification due to the Gaussian contribution diminishes for very large t0-values until it vanishes, and we retrieve the value $g \simeq 2$ of the Lorentzian line shape. This behavior is attributed to small wings of the Gaussian profile (see SM 1.2) that limit the contribution to a narrow spectral range close to the resonance wavelength, in which saturation at the blackbody spectral radiance occurs. The Lorentzian contribution dominates thus at very large t0-values, according to the large Lorentzian line wings (see SM 1.2).

The exponential error growth associated to the line-center measurement (see Fig. 2) is only observed for $w_{ap} \ll w_{sd}$. With increasing apparatus spectral width, the saturation of I_0 (see Fig. 1), and there with the exponential error growth, are shifted towards larger τ_0 values.

In typical conditions of LIBS experiments, spectral lines have a Doppler width of a few pm, and a Stark width ranging from picometers to nanometers. Thus, in most cases, the error growth factor is situated between the g-values of the pure Lorentzian profile and those observed for profiles with Gaussian contribution w_G/w_L ¼ 3 (see Fig. 2). The error of the line-integrated intensity if thus increased moderately by $g \simeq 2$ for $\tau_0 >> 1$.

As the amount of absorption depends on the spectral line width and the plasma size along the line of sight, the analytical measurement error is increased by the contributions of Δw_{sd} and ΔL, when self-absorbed lines are used [see eq (10)]. The plasma diameter can be estimated from fast plume imaging [19] or deduced from the line intensity ratio of self absorbed lines having significantly different optical thickness [20]. In both cases, the measurement accuracy is moderate and an error ΔL of about 10% is expected in the best case.

The spectral line width w_{sd} can be either computed or deduced from the measured width, and the associated error is thus given by the most precise of both values (see SM 1.4). When the apparatus spectral width w_{ap} and broadening due to self-absorption w_{sa} are small compared to the Stark width w_s, $w_{sd} \simeq w_s$ can be deduced with an accuracy close to accuracy of the measured width Δw_m, estimated to x 5%. In the opposite case, when $w_{sd} < w_{ap}, w_{sa}$, the computed spectral line width is more accurate than the measured value. However, Δw_{sd} is large due to large errors associated to the Stark broadening parameter Dus and the electron density Δn_e. Both errors are of about 10% in the best case, and most frequently of about 20% or larger, as accurate Stark broadening parameters are missing for many transitions.
Thus, compared to the optically thin case, analytical measurements with self-absorbed lines [eq (10)] are affected by three supplementary error contributions: the increase of the error associated to the intensity measurement [eq (11)], the uncertainty associated to the line width (see SM 1.4), and the error associated to the plasma diameter along the line of sight.

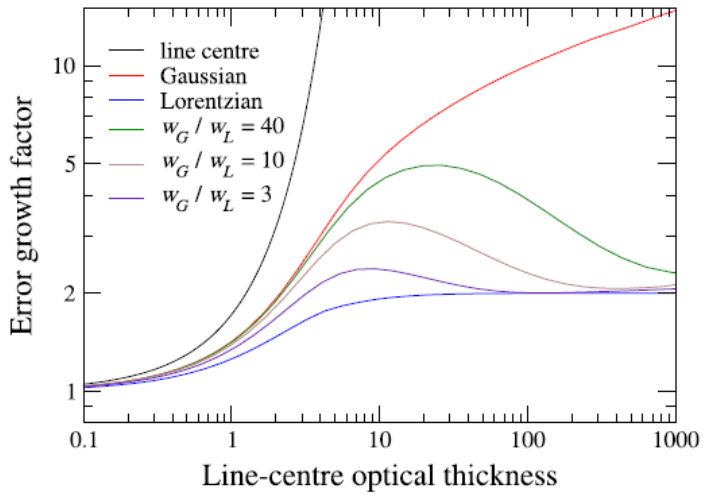

Fig. 2. Error growth factor vs τ_0 computed according eq (11) for I_0-measurements (black curve) and I_{line}-measurements of line profiles with different ratios of Gauss width w_G over Lorentz width w_L (colored curves).

2.2. Experimental section

2.2.1. LIBS setup

The experiments were carried out in experimental conditions that enable accurate modeling of the plasma emission spectrum [21,22]. Laser ablation was produced with a frequency-quadrupled Nd:YAG laser, delivering ultraviolet (266 nm) pulses of 4 mJ energy and 4 ns duration. The beam was focused to a spot of 100 μm diameter onto the sample surface, leading to a laser fluence of about 70 J cm^{-2}. The sample was placed on a motorized sample holder in a vacuum chamber that was filled with argon at 5×10^4 Pa pressure.

Optical emission spectroscopic measurements were performed by imaging the plasma with two lenses of 150 and 35 mm focal lengths onto the entrance of an optical fiber of 600 μm core diameter. The fiber was coupled to the entrance of an echelle spectrometer with a resolving power of 1×10^4. Photon detection was ensured using an intensified charge-coupled device matrix detector. The apparatus spectral width and the apparatus response were measured as functions of wavelength with appropriate calibrated lamps.

The spectra were recorded with a delay of 400 ns between the laser pulse and the detector gate. The gate width was set to 200 ns. To enhance the signal-to-noise ratio, data acquisition was performed by averaging over 200 ablation events, applying a single pulse on each irradiation site. The irradiation sites were separated by a distance of 150 μm.

The sample was a Si/Ge binary alloy thin film of $\simeq$ 50 nm average thickness, deposited on an alumina substrate of 25×60 mm^2 area. The film was deposited via so-called "combinatorial" pulsed laser deposition [23] to obtain a compositional gradient in the longitudinal direction with a variation of the Ge atomic fraction from 10% to 80%. The LIBS spectra were recorded for different longitudinal positions separated by a distance of 5 mm by moving the sample in the orthogonal direction, in which the composition is almost constant (see SM 2.1).

2.2.2. Computational details

The calculation of the spectral radiance according to eq (1) is implemented in an iterative measurement procedure that allows us to deduce the plasma properties including the elemental composition from the best agreement between measured and computed spectra [20]. The procedure consists of two main loops of iteration. The principal loop includes the successive measurements of electron density, plasma temperature, elemental fractions, and plasma size along the line of sight. For each measurement, the corresponding parameter is varied in order to find the best agreement between the computed and measured spectra in the wavelength ranges of the relevant atomic or ionic transitions. The calculations include the precise description of the spectral line profile, considering the dominating line broadening effects, namely Doppler and Stark broadening. As the probe depth was larger than the film thickness, the compositional measurements included the elements of both the thin film and the substrate. The spectroscopic data were taken from common databases and from literature (see SM 1.5).

3. Results and discussion

Accurate plasma diagnostics were performed using multiple transitions from both alloy-composing elements (see details in SM 2.2). The plasma properties listed in Table 1 were found to be independent of the measurement location on the sample surface, and thus independent of the elemental composition of the thin film.

Table 1. Electron density n_e, plasma temperature T, and plasma diameter along the line of sight L, deduced from the spectra analysis (see SM 2.2).

parameter (unit)	value	relative error
n_e (cm^{-3})	3.3×10^{17}	20%
T (K)	13100	2%
L (mm)	0.3	20%

To validate the prediction of the analytical measurement error according to eqs (10), (11) and (11)), two isolated germanium transitions of significantly different optical thicknesses were investigated. Prior to the analysis, their Stark broadening parameters were measured (see SM 2.3).

Measured and computed line profiles of both transitions are displayed in Fig. 3 for different Ge-fractions. For the weakly self-absorbed Ge 326.95 nm line (a), the intensity increases linearly with the Ge-fraction, whereas the line width augments only slightly (see Table S3). Contrarily, the strongly self-absorbed Ge 303.91 nm line (b) is characterized by a saturation-like intensity raise, and a stronger increase of line width with the Ge-fraction.

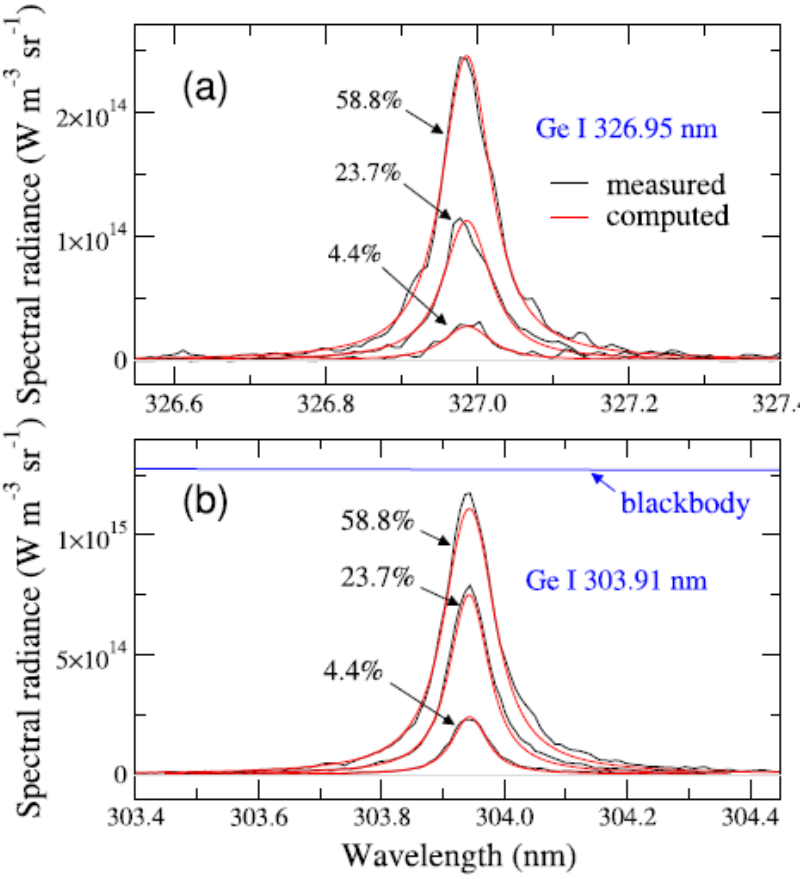

Fig. 3. Measured and computed spectral radiance of weakly (a) and strongly (b) self-absorbed lines. The measurements were performed for different locations on the sample surface, corresponding to different Ge-fractions within the thin film.

Both transitions have line widths more than two times larger than the apparatus width. Apparatus broadening is therefore moderate, and the measured line-center intensity is according to eq (3) close to the spectral radiance at

the resonance wavelength [$I_0 \simeq B_\lambda(\lambda_0)$]. Thus, the I_0-value of the Ge 303.91 nm transition approaches the blackbody spectral radiance for the largest Ge-fraction, as predicted by eq (1) for $\tau_0 = 2.6$ (see Fig. 1).

For both transitions, the Stark width is more than 20 times larger than the Doppler width. The dependence of the line-integrated intensity on τ_0 is therefore close to that of the Lorentzian profile (see Fig. 1). Accordingly, a significant error growth due to self-absorption is expected for analytical measurements exploiting the line-center intensity, whereas a moderate error increase is expected for measurements using the line-integrated intensity.

To validate the theoretical predictions, the measured and the computed line-center and line-integrated intensities are displayed in Fig. 4 as functions of the Ge atomic number density.

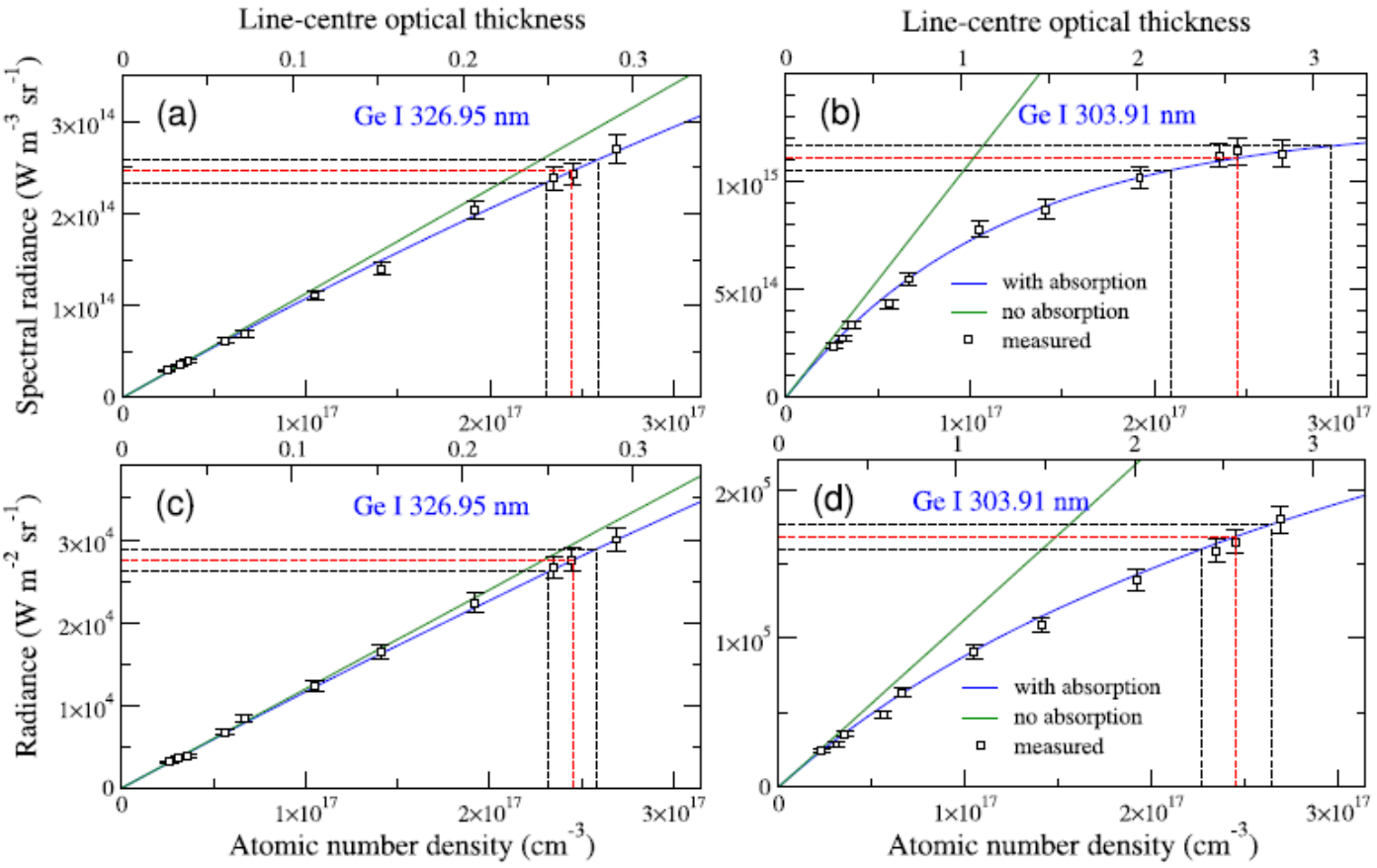

Fig. 4. Line-center spectral radiance (a,b) and line-integrated radiance (c,d) as functions of the Ge atomic number density and τ_0 (secondary *x*-axis) for weakly (a,c) and strongly (b,d) self-absorbed lines. The blue and green curves are the line intensities computed for a uniform plasma in LTE considering and ignoring self-absorption, respectively. The analytical measurement error is indicated for an intensity measurement error of 5% (dashed lines). (For interpretation of the references to color in this figure legend, the reader is referred to the Web version of this article.)

For the weakly self-absorbed Ge 326.95 nm transition, both I_0 (a) and I_{line} (c) show an almost linear increase with n_A. The error growth factor is thus close to unity (see Table 2). Nevertheless, the spectral radiance is notably reduced with respect to the optically thin case. The accurate calculation of the spectral radiance requires therefore the precise values of the line width and the plasma diameter, and the analytical error has contributions from Δw_{sd} and ΔL according to eq (10).

Table 2. Uncertainties associated to the Ge-fraction measurement for two transitions and three measurement locations (labelled 11, 6 and 2): atomic fraction C, line-center optical depth τ_0, weight factor $1-e^{-}(-\tau_0)$[see eq (10)], and line width error $\Delta w_{sd}/w_{sd}$. The intensity measurement error $\Delta I/I$, the associated error growth factor g, and the errors of atomic number density $\Delta n_A/n_A$ and atomic fraction $\Delta C/C$ are given for line-center (subscript 0) and line-integrated intensity (subscript *line*) measurements (see details in SM 1.4 and SM 2.5).

					I_0 measurement					I_{line} measurement				
transition	meas	C(%)	τ_0	$1-e^{-\tau_0}$	$\frac{\Delta w_{sd}}{w_{sd}}$	$\frac{\Delta I_0}{I_0}$	g_0	$\frac{\Delta n_A}{n_A}$	$\frac{\Delta C}{C}$	$\frac{\Delta w_{sd}}{w_{sd}}$	$\frac{\Delta I_{line}}{I_{line}}$	g_{line}	$\frac{\Delta n_A}{n_A}$	$\frac{\Delta C}{C}$
Ge I 303.91	11	10.0	0.25	0.22	8	5	1.14	13	14	8	5	1.06	13	14
	6	36.5	1.12	0.67	7	5	1.84	20	14	7	5	1.27	19	13
	2	80.2	2.6	0.93	12	5	4.84	32	7	6	5	1.55	22	5
Ge I 326.95	11	10.0	0.02	0.02	6	5	1.01	9	11	6	5	1.01	9	11
	6	36.5	0.11	0.11	7	5	1.06	10	9	7	5	1.03	10	9
	2	80.2	0.26	0.23	7	5	1.14	13	4	7	5	1.07	13	4

For the strongly self-absorbed Ge 303.91 nm transition, the measured line-center intensity (b) is shown to follow the saturation behavior according to eq (1). The measurement error increases thus rapidly with τ_0. Assuming an intensity measurement error of 5%, we deduce from the plotted data a measurement error of about 20% for $\tau_0 = 2.6$, in close agreement with the error growth factor $g_0 = 4.8$ obtained from eq (12) for the case of negligible apparatus broadening (see Table 2).

The saturation behavior is not observed for the line-integrated radiance of the Ge 303.91 nm transition (d) that is shown to increase with a reduced and almost constant slope in the range of large n_A (large τ_0) values, in agreement with the predicted I_{line}-growth for a pure Lorentzian line shape (see Fig. 1). Accordingly, the error growth is moderate, and we deduce geometrically a measurement error of about 8% for $\tau_0 = 2.6$, in agreement with the error growth by a factor of 1.6 predicted for the Lorentzian line shape (see Fig. 2).

The total increase of the analytical error, including the contributions Δw_{sd} and ΔL, is illustrated by the values $\Delta n_A/n_A$ and $\Delta C/C$ given in Table 2 for both lines and different Ge-fractions. Here, the $\Delta C/C$-values are misleading as the error diminishes with the Ge-fraction according to its large variation from 10% to 80% (see SM 1.7). We therefore refer to the analytical error expressed by $\Delta n_A/n_A$ that is shown to rise moderately from 9% to 13% when τ_0 increases from 0.02 to 0.26 (Ge 326.95 nm). In this regime of weak self-absorption, the error rise is equal for I_0- and I_{line}-measurements. A significantly larger $\Delta n_A/n_A$-increase from 13% to 22% is observed for I_{line}-measurements with Ge 303.91 nm according to the τ_0-raise from 0.25 to 2.6. The error increase is even enhanced from 13% to 32% for I_0-measurements.

4. Conclusion

The presented results show that the analytical measurement error due to self-absorption in calibration-free LIBS critically depends on the way the line intensity is measured and on the spectral line profile. As the line-center spectral radiance of strongly self-absorbed lines saturates at the blackbody spectral radiance, line-center intensity measurements lead to an exponential error growth with the optical thickness. With increasing apparatus broadening, the saturation behavior is shifted towards larger optical thickness. For line-integrated intensity measurements, the error growth due to self-absorption critically depends on the line shape. The largest error growth occurs for the Gaussian line profile wheras a moderate error increase by a factor ≤2 is expected for the Lorentzian profile. For mixed line shapes with significant Gaussian contribution, the error growth is increased compared to the pure Lorentzian shape, but this increase only occurs in a limited range of optical thickness.

As line broadening in LIBS plasmas is typically dominated by the Stark effect, the increase of the analytical measurement error due to the intensity measurement is moderate. However, the amount of absorption depends on line width and

plasma size, that are mostly known with moderate or low accuracy. The associated errors may thus present the principal error source of analytical measurements with self-absorbed spectral lines, if the model of the uniform equilibrium plasma is valid.

In the case of spatially non-uniform LIBS plasmas, the presented error evaluation still holds, if the appropriate model is applied. The analytical error is then obtained from the error evaluation of each plasma volume, characterized by its proper thermodynamic state.

CRediT authorship contribution statement

Aya Taleb: Investigation, Formal analysis, Writing – review & editing. **Vincent Motto-Ros:** Investigation, Writing – review & editing. **Mauro J. Carru:** Investigation, Writing – review & editing. **Emanuel Axente:** Resources, Validation, Writing – review & editing. **Valentin Craciun:** Resources, Validation, Writing – review & editing. **Frédéric Pelascini:** Conceptualization, Resources, Formal analysis. **Jörg Hermann:** Conceptualization, Methodology, Investigation, Data curation, Writing – original draft, Supervision, Writing – review & editing.

Declaration of competing interest

The authors declare that they have no known competing financial interests or personal relationships that could have appeared to influence the work reported in this paper.

Acknowledgments

The research leading to these results has received funding from ANRT (Association Nationale de la Recherche et de la Technology, CIFRE contract No. 2017/1219) and from LASERLAB-EUROPE (Grant Agreement No. 284464, European Union's Horizon 2020 research and innovation programme). E.A. and V.C. acknowledge the financial support from the Romanian NUCLEU project.

Appendix A. Supplementary data

Supplementary data to this article can be found online at https://doi.org/10.1016/j.aca.2021.339070.

References

1) R.D. Cowan, G.H. Dieke, Self-absorption of spectrum lines, Rev. Mod. Phys. 20 (1948) 418e455.

2) J. Hermann, C. Boulmer-Leborgne, D. Hong, Diagnostics of the early phase of an ultraviolet laser induced plasma by spectral line analysis considering self- absorption, J. Appl. Phys. 83 (2) (1998) 691e696.

3) T. Takahashi, B. Thornton, Quantitative methods for compensation of matrix effects and self-absorption in laser induced breakdown spectroscopy signals of solids, Spectrochim. Acta Part B At. Spectrosc. 138 (2017) 31e42.

4) V. Lazic, R. Barbini, F. Colao, R. Fantoni, A. Palucci, Self-absorption model in quantitative laser induced breakdown spectroscopy measurements on soils and sediments, Spectrochim. Acta Part B At. Spectrosc. 56 (2001) 807e820.

5) D. Bulajic, M. Corsi, G. Cristoforetti, S. Legnaioli, V. Palleschi, A. Salvetti, E. Tognoni, A procedure for correcting self-absorption in calibration-free laser-induced breakdown spectroscopy, Spectrochim. Acta Part B At. Spec- trosc. 57 (2002) 339e353.

6) J.D. Pedarnig, P. Kolmhofer, N. Huber, B. Praher, J. Heitz, R. Roessler, Element analysis of complex materials by calibration-free laser-induced breakdown spectroscopy, Appl. Phys. Mater. Sci. Process 112 (2013) 105e111.

7) M. Dell'Aglio, M. Lopez-Claros, J.J. Laserna, S. Longo, A. De Giacomo, Stand-off laser induced breakdown spectroscopy on meteorites: calibration-free approach, Spectrochim. Acta Part B At. Spectrosc. 147 (2018) 87e92.

8) I.B. Gornushkin, T. Volker, A.Y. Kazakov, Extension and investigation by nu- merical simulations of algorithm for calibration-free laser induced breakdown spectroscopy, Spectrochim. Acta Part B At. Spectrosc. 147 (2018) 149e163.

9) J.J. Maali, S.V. Shabanov, Error analysis in optimization problems relevant for calibration-free laser-induced breakdown spectroscopy, J. Quant. Spectrosc. Radiat. Transf. 222 (2019) 236e246.

10) N. Konjevic, Plasma broadening and shifting of non-hydrogenic spectral lines: present status and applications, Phys. Rep. 316 (1999) 339e401.

11) E. Tognoni, G. Cristoforetti, S. Legnaioli, V. Palleschi, A. Salvetti, M. Mueller, U. Panne, I. Gornushkin, A numerical study of expected accuracy and precision in calibration-free laser-induced breakdown spectroscopy in the assumption of ideal analytical plasma, Spectrochim. Acta Part B At. Spectrosc. 62 (2007) 1287e1302.

12) T. Li, Z. Hou, Y. Fu, J. Yu, W. Gu, Z. Wang, Correction of self-absorption effect in calibration-free laser-induced breakdown spectroscopy (CF-LIBS) with blackbody radiation reference, Anal. Chim. Acta 1058 (2019) 39e47.

13) J. Hou, L. Zhang, Y. Zhao, Z. Wang, Y. Zhang, M.A.W. Dong, W. Yin, L. Xiao, S. Jia, Mechanisms and efficient elimination approaches of self-absorption in LIBS, Plasma Sci. Technol. 21 (2019), 034016 1e15.

14) F. Rezaei, G. Cristoforetti, E. Tognoni, S. Legnaioli, V. Palleschi, A. Safi, A review of the current analytical approaches for evaluating, compensating and exploiting self-absorption in laser induced breakdown spectroscopy, Spectrochim. Acta Part B At. Spectrosc. 169 (2020) 105878, 1e25.

15) K. Touchet, F. Chartier, J. Hermann, J. Sirven, Laser-induced breakdown self- reversal isotopic spectrometry for isotopic analysis of lithium, Spectrochim. Acta Part B At. Spectrosc. 168 (2020), 105868 1e7.

16) J. Cooper, Plasma spectroscopy, Rep. Prog. Phys. 29 (1966) 35e130.

17) H.R. Griem, Plasma Spectroscopy, Academic, New York, 1964.

18) I.B. Gornushkin, J.M. Anzano, L.A. King, B.W. Smith, N. Omenetto, J.D. Winefordner, Curve of growth methodology applied to laser-induced plasma emission spectroscopy, Spectrochim. Acta Part B At. Spectrosc. 54 (1999) 491e503.

19) J. Hermann, E. Axente, V. Craciun, A. Taleb, F. Pelascini, Evaluation of pressure in a plasma produced by laser ablation of steel, Spectrochim. Acta Part B At. Spectrosc. 143 (2018) 63e70.

20) C. Gerhard, J. Hermann, L. Mercadier, L. Loewenthal, E. Axente, C.R. Luculescu, T. Sarnet, M. Sentis, W. Viol, Quantitative analyses of glass via laser-induced breakdown spectroscopy in argon, Spectrochim. Acta Part B At. Spectrosc. 101 (2014) 32e45.

21) J. Hermann, D. Grojo, E. Axente, C. Gerhard, M. Burger, V. Craciun, Ideal ra- diation source for plasma spectroscopy generated by laser ablation, Phys. Rev. E 96 (2017), 053210, 1e6.

22) J. Hermann, E. Axente, F. Pelascini, V. Craciun, Analysis of multi-elemental thin films via calibration-free laser-induced breakdown spectroscopy, Anal. Chem. 91 (2019) 2544e2550.

23) H.M. Christen, S.D. Silliman, K.S. Harshavardhan, Continuous compositional- spread technique based on pulsed-laser deposition and applied to the growth of epitaxial films, Rev. Sci. Instrum. 72 (2001) 2673e2678.